Pergamon

Geochimica et Cosmochimica Acta, Vol. 65, No. 24, pp. 4589–4596, 2001

0016-7037/01 $20.00 + .00

PII S0016-7037(01)00740-2

Determination of the $^{36}Ar/^{38}Ar$ isotopic abundance ratio of the solar wind using SOHO/CELIAS/MTOF

JAMES M. WEYGAND,[1,*,†] FRED M. IPAVICH,[2] PETER WURZ,[1] JOHN A. PAQUETTE,[2] and PETER BOCHSLER[1]

[1]Physikalisches Institut, Universität Bern, Bern, Switzerland
[2]Department of Physics, University of Maryland, MD, USA

(*Received November* 8, 2000; *accepted in revised form June* 25, 2001)

Abstract—This study is on the first direct measurements of the $^{36}Ar/^{38}Ar$ isotopic ratio in both the interstream (IS)-associated and coronal hole (CH)-associated solar wind. Two summed mass spectra are compiled for each solar wind region using the Mass Time-Of-Flight (MTOF) sensor of the Charge, Element, and Isotope Analysis System (CELIAS) instrument on the Solar and Heliospheric Observatory (SOHO) spacecraft. A detailed analysis of over 9.2 d of nonconsecutive IS-associated solar wind speed (395 ± 25 km/s) places the $^{36}Ar/^{38}Ar$ ratio at 5.6 ± 0.7. A similar analysis for a CH-associated solar wind speed (525 ± 25 km/s), with ~22.8 nonconsecutive days of CH-associated solar wind speed data, derived a similar $^{36}Ar/^{38}Ar$ ratio of 5.5 ± 0.6. The error associated with these measurements is essentially the instrumental uncertainty. Both the solar wind $^{36}Ar/^{38}Ar$ isotopic ratios found in this study are consistent with the terrestrial $^{36}Ar/^{38}Ar$ ratio as well as previous reported ratios for solar wind examined in this study. A comparison of these results suggests little or no isotopic fractionation occurring between the two solar wind regimes. This study presents the results in the context of solar wind fractionation models and in relation to experimental evidence derived from in situ observations on refractory elements.

1. INTRODUCTION

Previous measurements of the $^{36}Ar/^{38}Ar$ ratio were obtained from terrestrial samples, meteorites, lunar soil samples, and the Apollo missions' foil experiments (Eberhardt et al., 1965; Cerutti, 1974; Eugster and Niedermann, 1988; Wieler, 1998). The purpose of these measurements is to obtain accurate information on the isotopic composition of the present-day solar atmosphere. Furthermore, because the Sun's central temperature has never been high enough to alter the isotopic composition of the heavy elements by nuclear reactions, and because the Sun represents 99.9% of the matter in the solar system, an accurate isotopic composition measurement probably also reflects the isotopic composition of the presolar nebula. The difficulty with the interpretation of most previous measurements is the exposure of these samples over long periods of time (i.e., millions to billions of years) to a variety of effects, which may have changed the stored $^{36}Ar/^{38}Ar$ ratio. These effects consist of sputtering due to energetic particles, diffusion losses, and possibly interstellar neutrals (galactic composition) which drift into the solar system and ultimately become implanted as pick-up ions (Wimmer-Schweingruber and Bochsler, 2000; Wimmer-Schweingruber, 2000). Until now the best temporal resolution of the $^{36}Ar/^{38}Ar$ ratio has been ~2 d obtained with the Apollo missions' foil experiments.

The purpose of this study is to determine the $^{36}Ar/^{38}Ar$ ratio with the CELIAS/MTOF sensor for both interstream (IS) and coronal hole (CH) associated solar wind. Unfortunately, the uncertainty for the ratio within this work is large and may never be as small as those from other techniques limited to the Earth's surface such as the surface oxidation technique used in the study of Becker and Pepin (1991), the closed system stepped etching technique used in the work of Becker et al. (1998), and the stepwise pyrolytic extraction technique used in the Pepin et al. (1999) research. However, we place limits on the variability of the $^{36}Ar/^{38}Ar$ ratio directly in the contemporary solar wind under different solar wind conditions, as opposed to previous investigations which determined the ratio indirectly from the solar wind and are limited to ground-based studies.

2. INSTRUMENTATION

Two sensors of the Charge, Element, and Isotope Analysis System (CELIAS) instrument on board the Solar and Heliospheric Observatory (SOHO) spacecraft are used to obtain data for this study. The first of these is the proton monitor, which determines the solar wind proton density, temperature, and velocity over the range from 170 to 1200 km/s within ±20° of the normal solar wind direction. This sensor is used to select appropriate solar wind intervals for this study (Ipavich et al., 1998).

The Mass Time-Of-Flight (MTOF) sensor of the CELIAS instrument is an isochronous time-of-flight mass spectrometer (Hovestadt et al., 1995) with a mass resolution $M/\Delta M$ of ~100 and a temporal resolution of 5 min. MTOF combines an electrostatic entrance system and an isochronous time-of-flight spectrometer with the carbon foil technique to obtain mass spectra from the solar wind for a mass range between 1 and 60 AMU. Figure 1 is a schematic of the MTOF sensor, where the wide-angle, variable energy/charge (WAVE) entrance system is in the upper part of the figure and the time-of-flight (VMASS) section lies below the WAVE entrance system. The WAVE section consists of three energy over charge selection chambers. The entrance system allows a large energy range of

* Author to whom correspondence should be addressed (jweygand@igpp.ucla.edu)
† *Present address:* Institute of Geophysics and Planetary Physics, Department of Earth and Space Sciences, University of California, Los Angeles, 3845 Slichter Hall, Los Angeles, CA 90095-1567, USA.

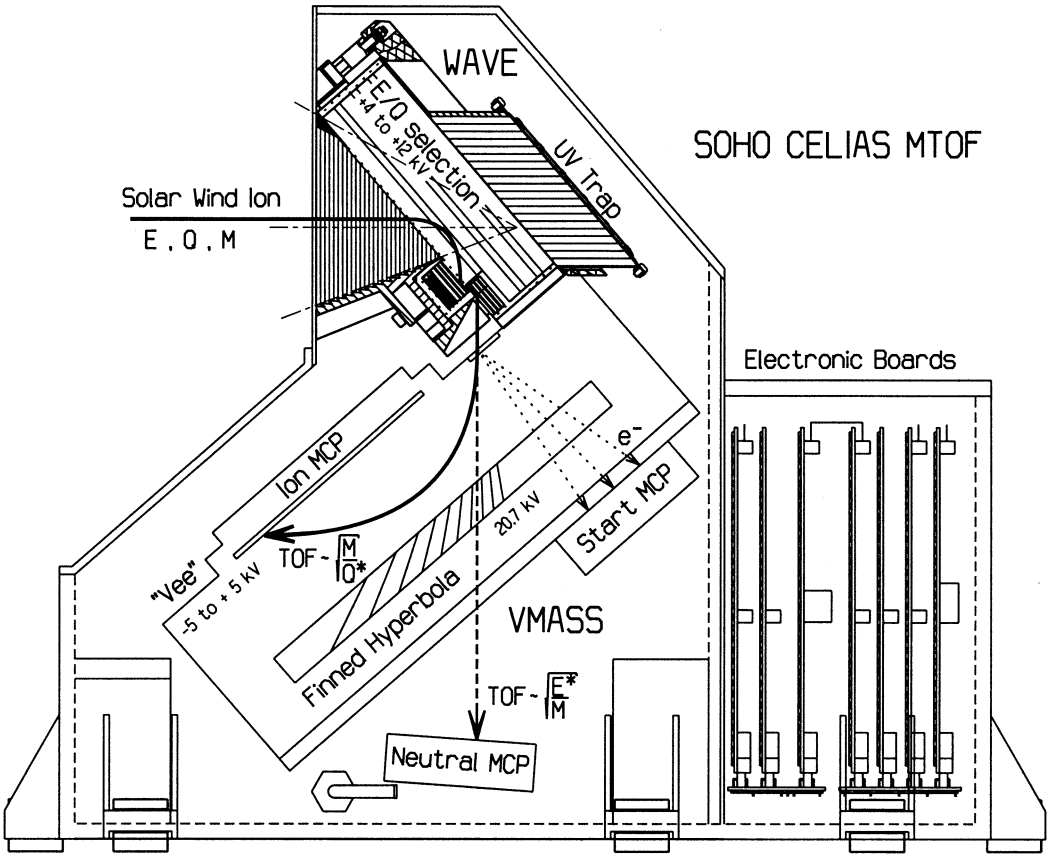

Fig. 1. Schematic of the CELIAS/MTOF sensor. The geometric dimensions of the CELIAS/MTOF sensor are 42 cm by 33.7 cm (length and height). Not shown is the width, which is 28.6 cm.

ions to enter the sensor through a wide angular acceptance cone. Particles, which pass through this region, cross through a carbon foil, which reduces their charge from some initial solar wind charge distribution (i.e., +8, +9, or +10 for argon) to neutral, +1, or +2, where the most probable ion charge is +1 according to the work of Bürgi et al. (1993). After the carbon foil, the ions follow a hyperbolic path to an ion multichannel plate (MCP) where they are recorded as counts.

3. PROCEDURE

The most important criterion for the data selection was a low signal-to-noise ratio (SNR). Unlike previous CELIAS/MTOF investigations, where the SNR is anywhere from ~4 to a few orders of magnitude, the SNR for argon was ~2.1 and just above 1.0 for ^{36}Ar and ^{38}Ar, respectively. To further complicate matters, additional constraints had to be imposed on the data set. The first of these constraints concerns binning of the data into either IS- or CH-associated solar wind. The IS-associated solar wind sample contains solar wind speeds between 370 km/s and 420 km/s, and the CH solar wind bin lies between 500 km/s and 550 km/s. These different solar wind regimes are defined based on the works of Aellig et al. (1999), Wurz et al. (1999), and Bochsler et al. (2000) for regions near the solar ecliptic plane. Figure 4 of the Aellig et al. (1999) study clearly shows the difference in solar wind composition versus the solar wind speed for the iron to oxygen ratio. The proton monitor, which is part of the CELIAS instrument on board the SOHO spacecraft, measures the speed of the solar wind, and the mass spectra will be obtained with the MTOF sensor. For the second constraint, the only instrument settings considered were those which allowed the two isotopes of argon to pass through the MTOF sensor in a very similar manner. While these two constraints largely restrict the total amount of data, they guarantee that ^{36}Ar and ^{38}Ar are treated nearly identically by the instrument. Figures 2 and 3 illustrate how the two isotopes "see" almost the same effective carbon foil area and how they have approximately the same total transmission probability through the VMASS portion of the sensor for the IS-associated solar wind bin and the CH-associated solar wind bin. Note that the figure of the effective carbon foil area for the CH-associated solar wind bin is not shown here. Calibration data for comparison exists only for ^{40}Ar, and the results of the programs agree well with the argon calibration data as well as with the calibration data for many other elements (results not shown here).

Figure 2 indicates the effective carbon foil area "seen" by an argon particle after crossing through only the WAVE portion of MTOF. The program used to determine the effective areas takes into account the speed of the solar wind, its kinetic temperature, the solar wind angle, the instrument settings, mass, and charge of the argon ions (Wurz, 1999). The dash-dot-dot-dot curve is the effective area for the ^{38}Ar isotope for various solar wind speeds, and the solid curve is the effective area for the ^{36}Ar isotope. The area between the first pair of vertical lines indicates the IS-associated solar wind speed range used in this study. Between these vertical segments, the argon curves differ at most by 3% for the two isotopes. This is indicated with the dashed line and the scale on the right of the figure. The second pair of vertical lines shows the CH-associated solar wind speed bin. Note that this plot is not accurate for the high-speed bin because different instrument settings are used for that bin. For the CH solar wind bin, the peak of the effective carbon foil area is shifted to the CH-associated bin for the appropriate instrument settings.

Figure 3 is a plot of the argon isotopes' total transmission through only the VMASS section of MTOF. This program also takes into

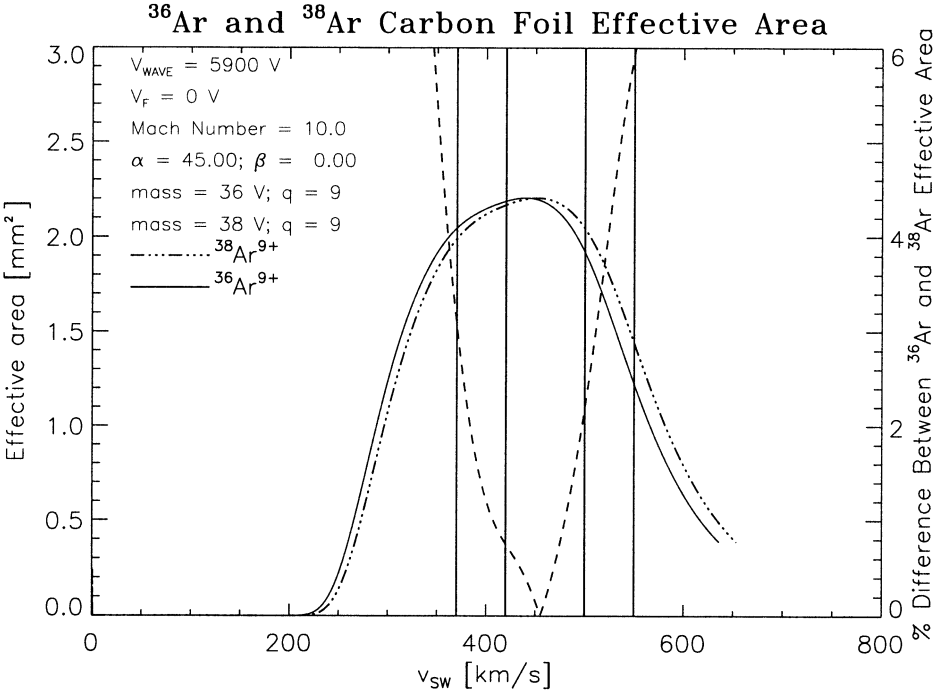

Fig. 2. The effective area of the carbon foil in the MTOF sensor from the point of view of the argon isotope. The approximate settings of the sensor are given in the upper left corner. The effective area of the ^{36}Ar isotope is indicated with the solid line and the ^{38}Ar isotope is represented with the dash-dot-dot-dot line. Within the solar wind interval of 370 km/s to 420 km/s, indicated with the two vertical lines, the argon curves differ at most by ~3%. Thus, the two argon isotopes pass through the entrance system of the MTOF sensor in almost the same manner. The second set of vertical lines indicates the CH-associated solar wind bin. Note that the effective carbon foil area differs for the CH bin due to different instrument settings.

account the speed of the solar wind, its kinetic temperature, the solar wind angle, the start efficiency of the electrons, stop efficiency of the electrons, effects of energy loss, angular spread, the instrument settings, mass, and charge of the argon ions (Wurz, 1999). The dashed curve is the transmission for the ^{38}Ar isotope over a range of solar wind values, and the solid curve is the transmission for the ^{36}Ar isotope for the same range. The dotted curve is the ratio of the ^{36}Ar isotope transmission to the ^{38}Ar isotope transmission. The scale for this curve is on the right side of the figure. The first pair of vertical lines indicates the IS-associated solar wind speed range. The second set of vertical lines indicates the transmission for the high-speed solar wind range. It should be clear from this plot why a narrow speed range was selected even though the SNR is low. At solar wind speeds less than 350 km/s and greater than 600 km/s, the total transmission in the VMASS portion of the instrument is low (i.e., less than 0.0003, which is ~75% below the maximum and an arbitrary cutoff). The solar wind range from 420 km/s to 500 km/s is avoided because this region is a mix between IS solar wind and CH solar wind (Aellig et al., 1999; Wurz et al., 1999). The solar wind bins from 370 km/s to 420 km/s and from 500 km/s to 550 km/s are used because they are IS- and CH-associated solar wind within the solar ecliptic plane, respectively (Aellig et al., 1999; Wurz et al., 1999), and have a ratio of the ^{36}Ar transmission value to the ^{38}Ar transmission value of nearly 1 (see the dotted curve in Fig.3 between the first set of vertical lines and the second set). The region from 550 km/s to 600 km/s is not used in this study in order to keep the two solar wind bins the same size, which prevents any potential bias, and because an examination of the spectra in this solar wind range shows that we obtain a poor mass spectrum for argon. This is most likely due to a high background resulting from more energetic particles entering the VMASS portion of the instrument and colliding with the fins of the hyperbola. The ratio of these two transmission curves in the CH-associated bin is ≅1.13 and for the IS-associated solar wind range of 370 km/s to 420 km/s the ratio of the curves is ≅0.91. A transmission ratio of 1 is desired because if the two transmission curves have a ratio of about unity, then essentially the two isotopes pass through the instrument in the same manner.

In summary, the intervals used were selected to be in "pure" IS- and CH-associated solar wind speed ranges where the total transmission was high, but the ratio of the two transmission curves is close to 1, and although the ratio is not unity, the ratio of the transmission curves is nearly a constant, which makes corrections to the argon isotopic ratio easier and more reliable. It is important to emphasize the balance between having IS- and CH-associated speed solar wind bins, obtaining enough counts for the mass spectra, and at the same time limit the amount of uncertainty in the measurement.

Table 1 lists the instrument settings required for the selection of data for the two different solar wind speed ranges. Again, these settings were selected to maximize the SNR, but at the same time minimize the difference in transmission.

Data from 1996 to the first half of 1999 were examined, and the selected mass spectra were summed together to make one total mass spectrum for each solar wind speed range. For the IS-associated solar wind, the summed spectra amounts to 9.2 d worth of data. For the CH-associated solar wind, the summed spectra is for 22.8 d worth of data. The top panel of Figure 4 shows the total mass spectrum for the IS-associated solar wind, and the top panel of Figure 5 displays the mass spectrum for the CH-associated solar wind, respectively. Within the spectrum seven mass peaks are visible, namely ^{34}S, ^{35}Cl, ^{36}Ar, ^{37}Cl, ^{38}Ar, ^{39}K, and ^{40}Ca. Along the x-axis is the channel number of the time-of-flight (TOF) MCP; along the y-axis is the total number of counts per channel; the thin black line indicates the raw data; and the thick curve is a 16-parameter Maximum Likelihood fit to the spectrum. Plotted with each raw data mass peak is an error bar to show the approximate uncertainty in the counts as well as the goodness of the fit. Error bars are not plotted for all channel numbers because the plot would become more difficult to read. The bottom part of each figure is a plot of the relative difference of the raw spectrum from the fit spectrum. It should be clear from the lower panel in the plot how good

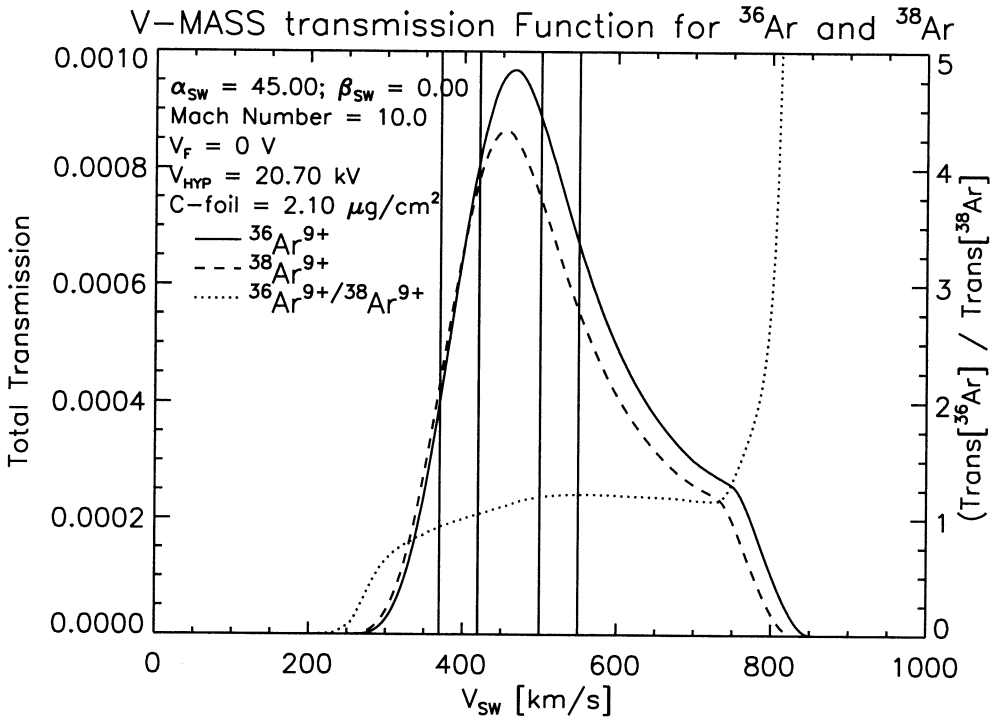

Fig. 3. Total transmission of the isochronous TOF mass spectrometer is plotted for the two argon isotopes investigated in this study. The approximate settings of the MTOF sensor and the general solar wind values are located in the upper left-hand corner. The effective area of the ^{36}Ar isotope is indicated with the solid line and the ^{38}Ar isotope is represented with the dash line. The two vertical lines on the figure's left side indicate the interval of 370 km/s to 420 km/s solar wind. The two vertical lines on the right side of the figure indicate the CH-associated solar wind bin. Thus, the two argon isotopes pass through the VMASS portion of the instrument in almost the same manner. The dotted curve indicates the transmission ratio of ^{36}Ar to ^{38}Ar with a ratio of nearly 1 in both solar wind bins.

the fit is, and relative difference variation above and below zero indicates that we are fitting with the proper fit function and the residues are just noise.

From the spectrum it is clear that the mass peaks are not symmetric, which is due to the asymmetry in the isochronous time of flight. More importantly, the shape of the peak is essentially the same for each mass peak. For this study, the asymmetric peak shape is considered to be the superposition of a Gaussian and two Lorentzians, one for the peak's left side (Γ_L) and the other for the right side (Γ_R). The Gaussian peak height (H_i) and width (σ) represent two parameters of the peak, and the widths of the Lorentzians represent two more. The fractional contribution of the Gaussian to the total peak shape is another free parameter, *f*, in this fit. There are seven mass peaks, hence, this is a total of 11 parameters.

The function for the total spectrum background in the argon mass peaks region is found by fitting the sites between the mass peaks. From this examination of the total spectrum background, the best fit for the background is determined to be a quadratic function, which is an additional three parameters to the entire spectrum fit.

Table 1. MTOF sensor instrumental settings for different solar wind bins.

Portion of MTOF sensor	IS solar wind (370 to 420 km/s)	CH solar wind (500 to 550 km/s)
Acceleration voltage (V_f)	0.0	0.0
Hyperbola voltage	20.7 kV	20.7 kV
Entrance system voltage	4.9 to 7.9 kV	8.0 to 12.4 kV
Minimum solar speed duration	300 s	300 s
North/south solar wind angle	±8°	±8°
Mach number	≥10.0	≥0.0

The final two parameters are related to the isochronous time of flight of the mass particles through the instrument. Because the time of flight in the mass spectrometer is proportional to the square root of the particle's mass, this proportionality is used to assign masses to the time-of-flight peaks in the spectrum according to the expression

$$T_i = (T_{40} - T_{offset}) \cdot \sqrt{\frac{m_i}{m_{40}}} \tag{1}$$

where T_i is the nominal time of flight of species *i* with nuclear mass m_i, T_{40} is the nominal time-of-flight position for the ^{40}Ca mass peak, and T_{offset} is a small, identical offset for each mass peak. ^{40}Ca was selected to fix all peaks' locations because it is the largest peak within this mass range. The two remaining free parameters are T_{offset} and T_{40}, which are used to fix the location of all seven mass peaks within the selected time-of-flight range.

The resulting equation for the Maximum Likelihood fit for the seven mass peaks is:

$$\mu(T) = \sum_{T_i>T,i=1}^{9} H_i \left[\left(\frac{\Gamma_L^2}{(T - T_i)^2 + \frac{\Gamma_L^2}{4}} \right) + f \cdot e^{-\frac{(T-T_i)^2}{2\sigma^2}} \right] + \sum_{T_i\le T,i=1}^{9} H_i \left[\left(\frac{\Gamma_R^2}{(T-T_i)^2+\frac{\Gamma_R^2}{4}} \right) + f \cdot e^{-\frac{(T-T_i)^2}{2\sigma^2}} \right] + b_0 + b_1 \cdot T + b_2 \cdot T^2 \tag{2}$$

where the parameters b_0, b_1, and b_2 are the zeroth, first, and second orders of the quadratic background.

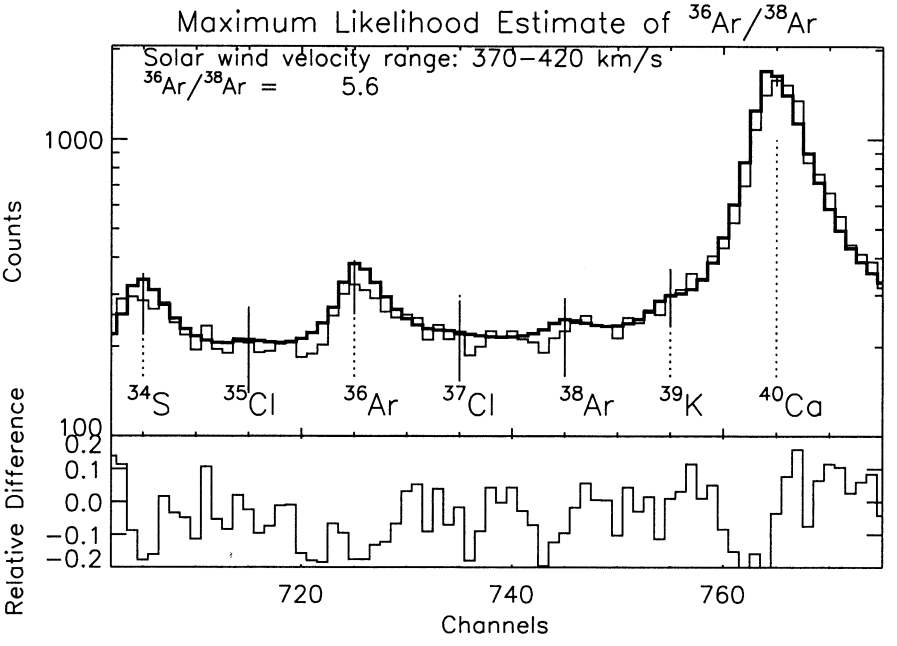

Fig. 4. The top panel shows the accumulated 5-min mass spectra between 1996 and 1999 for the IS-associated solar wind range of 370 km/s to 420 km/s. The thin black line represents the raw data, and the thick black line is the Maximum Likelihood fit of the ^{34}S, ^{35}Cl, ^{36}Ar, ^{37}Cl, ^{38}Ar, ^{39}K, and ^{40}Ca peaks. Along the y-axis are the counts, along the x-axis is the TOF channel, and each isotope is labeled above or underneath each peak. The dotted line indicates the peak's position. Plotted on each raw data mass peak is one error bar to indicate to the reader the uncertainty in the counts. The bottom panel is a plot of the relative difference [(raw − fit)/raw] of the raw spectrum from the fit spectrum. It should be clear from the lower panel how good the fit is, and variation of the relative difference above and below zero indicates that we are not consistently fitting above or below the raw data.

4. RESULTS AND DISCUSSION

Both values of the ^{36}Ar to ^{38}Ar ratio for the IS-associated solar wind and CH-associated solar wind are shown at the bottom of Table 2 in comparison with data from other works. The ratio for this study represents the ratio of the areas under the curve for six channels. Our values are consistent with the

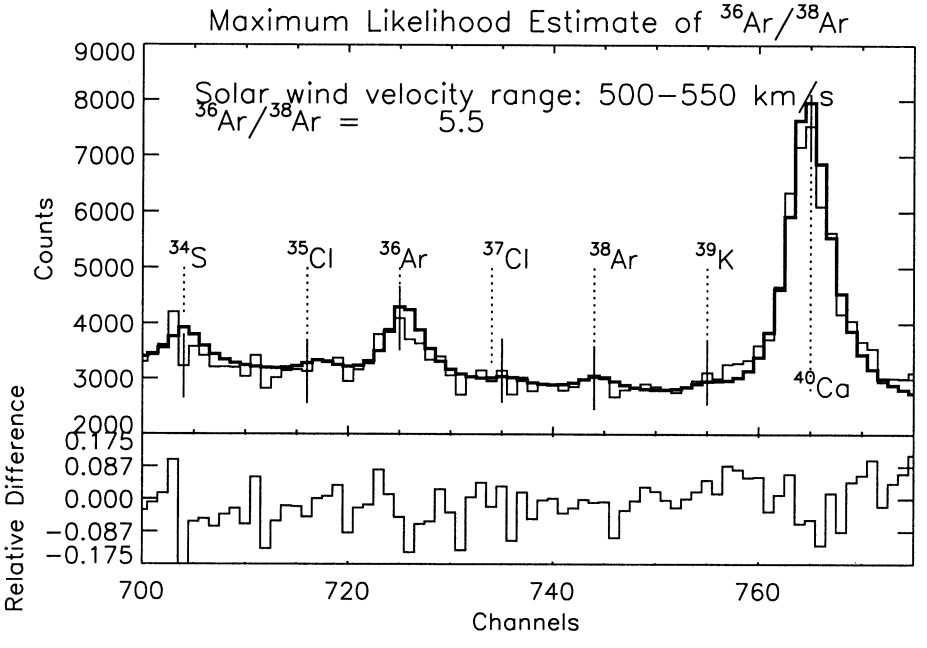

Fig. 5. Same as Figure 4, but for solar wind speeds from 500 km/s to 550 km/s and using a linear scale.

Table 2. Comparison of $^{36}Ar/^{38}Ar$ ratios from samples.

Sample	Measured value	Reference
Terrestrial atmosphere	5.32	Nier, 1950
Terrestrial mantle	5.8 ± 0.1	Pepin, 1998
Surveyor 3 strut	5.41 ± 0.20	Warasila and Schaeffer, 1974
Kapoeta achondrite meteorite surface of grains	5.58 ± 0.03	Becker et al., 1998
Lunar soil (ilmenite and pyroxenes)	5.77 ± 0.08	Benkert et al., 1993
Apollo foils	5.3 ± 0.3	Cerutti, 1974
Slow solar wind	5.6 ± 0.7	This work
Fast solar wind	5.5 ± 0.6	This work

previously accepted solar wind results of the Cerutti (1974) study with the Apollo foils (see Table 2) and with the ratio from the works of Nier (1950) for the terrestrial atmosphere, Warasila and Schaeffer (1974) using the Surveyor 3 strut, Pepin (1998) for the terrestrial mantle, Becker et al. (1998) on meteorite grains irradiated at the surface of the parent body of the Kapoeta achondrite meteorite, and Benkert et al. (1993) for lunar soils.

The ^{36}Ar to ^{38}Ar ratio of this study differs the most from the terrestrial ^{36}Ar to ^{38}Ar ratio, but our values are consistent with the terrestrial $^{36}Ar/^{38}Ar$ ratio as well as those in Table 2. The difference with respect to the terrestrial argon ratio is 6% and 4% for the IS- and CH-associated solar wind, respectively, and the difference is not significant (i.e., it is a 0.5 sigma difference).

The large uncertainty estimated for our values is the result of the quadratic sum of the independent relative uncertainties. The background is estimated to have a relative uncertainty ($\sqrt{n}/n$ where n is the counts of the background) of 7% for the IS-associated solar wind and 2% for the CH-associated solar wind. The instrumental relative uncertainty for the WAVE portion of MTOF according to Figure 2 is approximately 3% for the IS-associated solar wind and ~4% for the CH-associated solar wind. The errors related to the counts represent the one sigma level. The instrumental relative uncertainty for the VMASS portion of MTOF according to Figure 3 is approximately 3% for the IS-associated solar wind and ~8% for the CH-associated solar wind, where the large relative uncertainty for the CH-associated solar wind bin is due to the large difference between the transmission curves (Fig. 3). The area under the IS-associated solar wind peaks has a relative uncertainty of approximately 3% and 8% for ^{36}Ar and ^{38}Ar, respectively, whereas for the area under the CH-associated solar wind peak we find ~1% and 4% relative uncertainty for ^{36}Ar and ^{38}Ar, respectively. This results in a total relative uncertainty of ~12% for the IS-associated solar wind value and ~10% for the CH-associated solar wind value. Unfortunately, these uncertainties are not expected to improve much with the addition of more MTOF data.

The uncertainty could only be moderately improved by further restricting the sensor settings and with the accumulation of a much larger number of spectra. This work is based on spectra covering a few weeks of solar wind flow. Investigations that involve the lunar soils, lunar meteorites, and other meteorites obtain values that are the result of an accumulation over a period of millions (or even billions) of years. These latter studies can not take into account an "uncertainty" due to statistical variation of the solar wind (i.e., changes in the $^{36}Ar/^{38}Ar$ ratio due to variations in the speed, sputtering, diffusion losses, and galactic contributions). Studies that involve the terrestrial mantle examine an inherited $^{36}Ar/^{38}Ar$ ratio, possibly from the presolar nebula (Pepin, 1998), but the purity of these samples is unclear. Reservations on this sample have been expressed in the studies of Kunz (1999) and evidence against the presence of a pure presolar nebula sample is presented in the Niedermann et al. (1997) work. Thus, one should keep in mind that in comparing the absolute errors given in Table 2, for the terrestrial mantle, lunar soils, lunar meteorites and other meteorites, these errors represent merely instrumental and experimental uncertainties and do not include statistical variations.

The Apollo solar wind foils, on the other hand, had exposure times from approximately 18.5 h to 45 h, which is less than the accumulation times of this study. The $^{36}Ar/^{38}Ar$ ratio obtained with these foils is approximately 5.3 ± 0.3, which is the average of the Apollo 12, 14, 15, and 16 missions (Cerutti, 1974). The $^{36}Ar/^{38}Ar$ ratio of this study is consistent with the average Apollo solar wind foil finding and with each value found on the separate Apollo missions, which is 5.3 ± 0.05 for the Apollo 12 mission, 5.2 ± 0.5 for the Apollo 14 mission, 5.2 ± 0.3 for the Apollo 15 mission, and 5.5 ± 0.4 for the Apollo 16 mission. During three of the four missions (Apollo 11, 12, and 16) the solar wind speeds are available and appeared to be quiet, between 320 km/s and 400 km/s (see http://nssdc.gsfc.nasa.gov/omniweb/). This range is similar to our IS-associated solar wind bin $^{36}Ar/^{38}Ar$ argon isotopic ratio.

The large $^{36}Ar/^{38}Ar$ uncertainty makes an analysis of the fractionation due to first ionization potential (FIP) difficult. A systematic and critical discussion of theoretical FIP models is beyond the scope of this study, but a brief look at the Bodmer and Bochsler (2000) model is done in this work. In the recent studies of Bodmer and Bochsler (2000) and Bochsler (2000), the role of coulomb collisions in minor ion acceleration is examined using a multifluid model. Within the model the behavior of the minor ions also depends upon their mass and charge through the interplay of wave acceleration, gravity, pressure gradients, electromagnetic fields, coulomb drag, and thermal diffusion. The result is an isotopic effect where the heavier isotopes of the heavy elements are depleted in the solar wind relative to protons, but this amounts to only a few percent at most in relation to a large He/H depletion factor.

Figure 6 illustrates the variation of $^{36}Ar/^{38}Ar$ isotopic ratio with He/H depletion (see the solid line). From this figure, it is clear that at most the decrease of the $^{36}Ar/^{38}Ar$ ratio is ~4% for a typical solar wind argon charge of 9^+ at a He/H depletion of

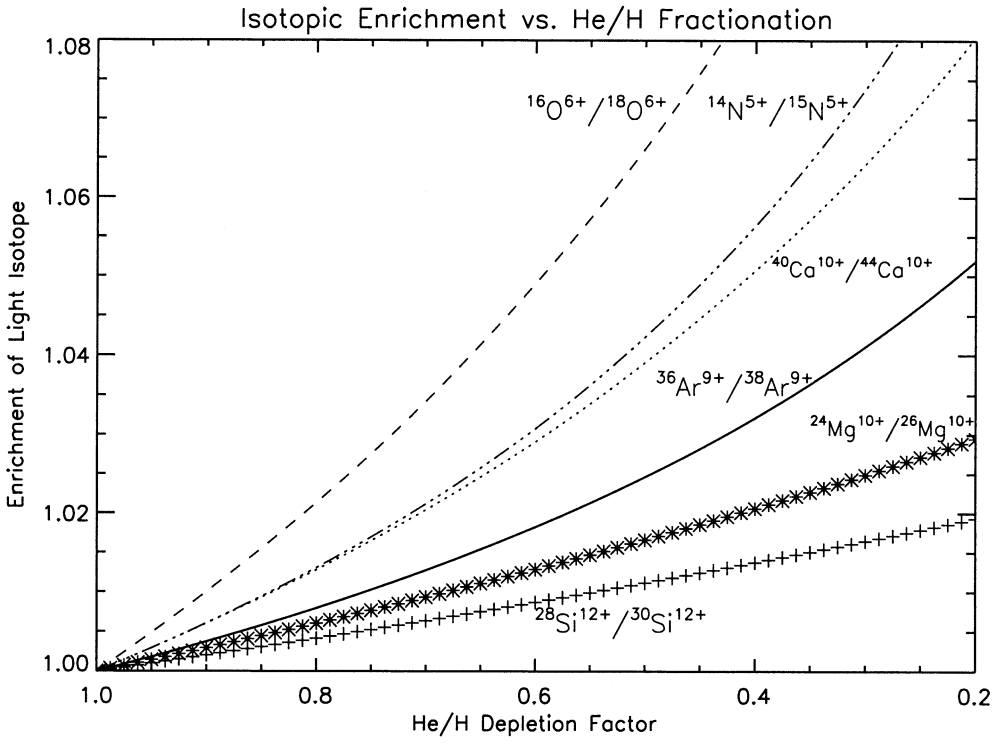

Fig. 6. This figure demonstrates the enrichment of the lighter isotope with respect to the depletion of helium to hydrogen derived from the Bodmer and Bochsler (2000) model. The solid line is the enrichment of ^{36}Ar to ^{38}Ar for a charge of +9, which is the expected charge of argon in a solar wind of temperature 1.2 MK; the dash line is the enrichment of the ^{16}O to ^{18}O for a charge of +6; the dash-dot-dot-dot line is the enrichment of the ^{14}N to ^{15}N for a charge of +5; the asterisk line is the enrichment of the ^{24}Mg to ^{26}Mg for a charge of +10; the "+" line is the enrichment of the ^{28}Si to ^{30}Si for a charge of +12; and the dotted line is the enrichment of the ^{40}Ca to ^{44}Ca for a charge of +10.

0.3. Within Figure 6 are the curves for several other isotopic ratios. Similar to the argon isotopic ratio curve, the others show an enrichment of the light isotope on the order of a few percent to ~10% for ^{16}O at a He/H of 0.3. The studies of Kallenbach et al. (1998) using Si, Ne, and Mg and Kucharek et al. (1998) using just Mg also indicate an enrichment of the light isotope (or a depletion of the heavy isotope according to the work of Kallenbach et al., 1998). The results of the Kallenbach et al. (1997) study for the Ne isotopic ratio alone, however, do not clearly show an enrichment of the light isotope. Whether the enrichment (or depletion) is really the case in those studies is not clear due to the large uncertainty associated with the measurements. Hence, the difference in the IS- and CH-associated solar wind argon isotopic ratios is consistent with the predictions of the Bodmer and Bochsler (2000) model for this study and previous works, but this difference is again insignificant in view of the large uncertainty of the $^{36}Ar/^{38}Ar$ isotopic ratios, and it could as well be that there is no systematic difference in the isotopic ratio between the IS- and CH-associated solar wind.

One last item to point out is the observation of ^{35}Cl and ^{37}Cl in Figure 5 (there are chlorine peaks in Figure 4, but they are not very large). MTOF provides the first direct observation of chlorine within the solar wind. The $^{35}Cl/^{37}Cl$ isotopic ratio was not calculated here because of the large uncertainty on the accumulated spectrum points.

5. CONCLUSION

The $^{36}Ar/^{38}Ar$ isotopic ratios for the IS- and CH-associated solar wind of this study are consistent with previously published values on the terrestrial mantle, lunar foils, lunar soils, and meteorites. The IS-associated solar wind $^{36}Ar/^{38}Ar$ isotopic ratio is determined to be 5.6 ± 0.7, and a value of 5.5 ± 0.6 is reported for the CH-associated solar wind $^{36}Ar/^{38}Ar$ isotopic ratio. The difference in the isotope ratios between the IS- and CH-associated speed solar wind samples can be explained by the Bodmer and Bochsler (2000) model on fractionation related to coulomb collisions. Unfortunately, this comparison is meaningless, because the uncertainty of two ratios is 10% or more. In addition to the first direct measurements of the $^{36}Ar/^{38}Ar$ isotopic ratios, the first direct solar wind observation is made of the two chlorine isotopes, ^{35}Cl and ^{37}Cl.

Acknowledgments—This work is supported by the Swiss National Science Foundation. CELIAS is a joint effort of five hardware institutions under the direction of the Max-Planck Institut für Extraterrestrische Physik (prelaunch) and the University of Bern (postlaunch). The University of Maryland was the prime hardware institution for MTOF, the University of Bern provided the entrance systems for MTOF, and the Technical University of Braunschweig provided the data processing unit. We would also like to thank Emma Salerno and Fritz Bühler for their helpful advice and productive discussions. We also thank Prof. R. Wieler and the other two referees for their helpful comments.

Associate editor: R. Wieler

REFERENCES

Aellig M. R., Hefti S., Grünwaldt H., Bochsler P., Wurz P., Ipavich F. M., and Hovestadt D. (1999) The Fe/O elemental abundance ratio in the solar wind as observed with SOHO/CELIAS/CTOF. *J. Geophys. Res.* **104,** 24769–24780.

Becker R. H. and Pepin R. O. (1991) Composition of solar wind noble gases released by surface oxidation of a metal separate from the Weston meteorite. *Earth Planet. Sci. Lett.* **71,** 55–68.

Becker R. H., Schlutter D. J., Rider P. E., and Pepin R. O. (1998) An acid-etch study of the Kapoeta achondrite: Implications for the argon-36/argon-38 ratio in the solar wind. *Meteor. Planet. Sci.* **33,** 109–113.

Benkert J.-P., Baur H. Signer P., and Wieler R. (1993) He, Ne, and Ar from the solar wind and solar energetic particles in lunar ilmenites and pyroxenes. *J. Geophys. Res.* **98,** 13147–13162.

Bochsler P. (2000) Abundances and charge states of particles in the solar wind. *Rev. Geophys.* **38,** 247–266.

Bochsler P., Ipavich F. M., Paquette J. A., Weygand J. M., and Wurz P. (2000) Determination of the abundance of aluminum in the solar wind. *J. Geophys. Res.* **105,** 12659–12666.

Bodmer R., and Bochsler P. (2000) Influence of Coulomb collisions on isotopic elemental fractionation in the solar wind acceleration process. *J. Geophys. Res.* **105,** 47–60.

Bürgi A., Gonin M., Oetliker M., Bochsler P., Geiss J., Lamy T., Brenac A., Andrä H. J., Roncin P., Laurent H., and Coplan M. A. (1993) Charge exchange of low-energy ions in thin carbon foils II: Results for ions of B, C, F, Ne, Na, Si, S, Cl, Ar, K, and Fe. *J. Appl. Phys.* **73,** 4130–4139.

Cerutti H. (1974) Die Bestimmung des Argons im Sonnenwind aus Messungen an den Apollo - SWC - Folien. Ph.D. thesis, University of Bern, Switzerland.

Eberhardt P., Geiss J., and Grögler N. (1965) Ueber die Verteilung der Uredelgase im Meteoriten Khor Temiki. *Tschermaks Min. u. Petr. Mitt.* **10,** 535–551.

Eugster O., and Niedermann S. (1988) Noble gasses in lunar meteorites Yamato-82192 and -82193 and history of the meteorites from the moon. *Earth Planet. Sci. Lett.* **89,** 15–27.

Hovestadt D., Hilchenbach H., Bürgi A., Klecker B., Laeverenz P., Scholer M., Grünwaldt H., Axford W. I., Livi S., Marsch E., Wilken B., Winterhoff P., Ipavich F. M., Bedini P., Coplan M. A., Galvin A. B., Gloeckler G., Bochsler P., Balsiger H., Fischer J., Geiss J., Kallenbach R., Wurz P., Reiche K.-U., Gliem F., Judge D. L., Hsieh K. C., Möbius E., Lee M. A., Managadze G. G., Verigin M. I., and Neugebauer M. (1995) CELIAS -Charge, Element and Isotope Analysis System from SOHO. *Solar Physics* **162,** 441–481.

Ipavich F. M., Galvin A. B., Lasley S. E., Paquette J. A., Hefti S., Reiche K.-U., Coplan M. A., Gloeckler G., Bochsler P., Hovestadt D., Grünwaldt H., Hilchenbach M., Gliem F., Axford W. I., Balsiger H., Bürgi A., Geiss J., Hsieh K. C., Kallenbach R., Klecker B., Lee M. A., Mangadze G. G., Marsch E., Möbius E., Neugebauer M., Scholer M., Verigin M. I., Wilken B., and Wurz P. (1998) The solar wind proton monitor on the SOHO spacecraft. *J. Geophys. Res.* **103,** 17205–17214.

Kallenbach R., Ipavich F. M., Bochsler P., Hefti S., Hovestadt D., Grünwaldt H., Hilchenbach M., Axford W. I., Balsiger H., Bürgi A., Coplan M. A., Galvin A. B., Geiss J., Gliem F., Gloeckler G., Hsieh K. C., Lee M. A., Livi S., Managadze G. G., Marsch E., Möbius E., Neugebauer M., Reiche K.-U., Scholer M., Verigin M. I., Wilken B., and Wurz P., (1997) Isotopic composition of solar wind neon measured by CELIAS/MTOF on board SOHO. *J. Geophys. Res.* **102,** 26895–26895.

Kallenbach R., Ipavich F. M., Kucharek H., Bochsler P., Galvin A. B., Geiss J., Gliem F., Gloeckler G., Grünwaldt H., Hefti S., Hilchenbach M., and Hovestadt D. (1998) Fractionation of Si, Ne, and Mg isotopes in the solar wind as measured by SOHO/CELIAS/MTOF. *Space Sci. Rev.* **85,** 357–370.

Kucharek H., Ipavich F. M., Kallenbach R., Bochsler P., Hovestadt D., Grünwaldt H., Hilchenbach M., Axford W. I., Balsiger H., Bürgi A., Coplan M. A., Galvin A. B., Geiss J., Gliem F., Gloeckler G., Hsieh K. C., Judge D. J., Klecker B., Lee M. A., Livi S., Managaze G. G., Managaze G., Marsch E., Möbius E., Neugebauer M., Ogawa H. S., Reiche K.-U., Scholer M., Verigin M. I., Wilken B., and Wurz P. (1998) Magnesium isotopic composition as observed with the CELIAS/MTOF experiment on the SOHO spacecraft. *J. Geophys. Res.* **103,** 26805–26812.

Kunz J. (1999) Is there solar argon in the Earth's mantle. *Nature* **399,** 649–650.

Niedermann S., Bach W., and Erzinger J. (1997) Noble gas evidence for a lower mantle component in MORBs from the southern East Pacific Rise: Decoupling of helium and neon. *Geochim. Cosmochim. Acta* **61,** 2697–2715.

Nier A. O. (1950) A redetermination of the relative abundances of isotopes of carbon, nitrogen, oxygen, argon, and potassium. *Phys. Rev.* **77,** 789–793.

Pepin R. O. (1998) Isotopic evidence for a solar argon component in the Earth's mantle. *Nature* **394,** 664–667.

Pepin R. O., Becker R. H., and Schlutter D. J. (1999) Irradiation records in regolith materials. I: Isotopic compositions of solar-wind neon and argon in single lunar grains. *Geochim. Cosmochim. Acta* **63,** 2145–2162.

Warasila R. L., and Schaeffer O. A. (1974) Trapped solar wind He, Ne, and Ar and energetic He in Surveyor 3. *Earth Planet. Sci. Lett.* **24,** 71–77.

Wieler R. (1998) The solar noble gas record in lunar samples and meteorites. *Space Sci. Rev.* **85,** 303–314.

Wimmer-Schweingruber R. F. (2000) Lunar soils: A long-term archive for the galactic environment of the solar system. Habilitation thesis, University of Bern, Switzerland.

Wimmer-Schweingruber R. F., and Bochsler P. (2000) Is there a record of interstellar pick-up ions in the lunar regolith? In *Acceleration and Transport of Energetic Particles Observed in the Heliosphere* (eds. R. A. Mewaldt J. R. Jokipii M. A. Lee E. Moebius, and T. H. Zurbuchen), pp. 270–273. AIP conference proceedings, Woodbury, NY.

Wurz P. (1999) Heavy ions in the solar wind: Results from SOHO/CELIAS/MTOF. Habilitation thesis, University of Bern, Switzerland.

Wurz P., Aellig M. R., Ipavich F. M., Hefti S., Bochaler P., Galvin A. B., Hilchenbach M., Gliem F., and Hovestadt D. (1999) The iron, silicon and oxygen abundance in the solar wind measured with SOHO/CELIAS/MTOF. *Phys. Chem. Earth* **24,** 421–426.